Metabolism Clinical and Experimental 96 (2019) 22–32

Contents lists available at ScienceDirect

Metabolism Clinical and Experimental

journal homepage: www.metabolismjournal.com

Basic Science

Lipoxygenase drives lipidomic and metabolic reprogramming in ischemic heart failure

Ganesh V. Halade *, Vasundhara Kain, Bochra Tourki, Jeevan Kumar Jadapalli

Division of Cardiovascular Disease, Department of Medicine, The University of Alabama at Birmingham, AL, United States

ARTICLE INFO

Article history:
Received 23 February 2019
Accepted 11 April 2019

Keywords:
Heart failure
Metabolic signaling
Leukocytes
Lipid mediators
Metabolites
Resolution of inflammation

ABSTRACT

Background: After myocardial infarction (MI), delayed progression or reversal of cardiac remodeling is a prime target to limit advanced chronic heart failure (HF). However, the temporal kinetics of lipidomic and systemic metabolic signaling is unclear in HF. There is no consensus on metabolic and lipidomic signatures that influence structure, function, and survival in HF. Here we use genetic knock out model to delineate lipidomic, and metabolic changes to describe the role of lipoxygenase in advancing ischemic HF driven by leukocyte activation with signs of non-resolving inflammation. Bioactive lipids and metabolites are implicated in acute and chronic HF, and the goal of this study was to define the role of lipoxygenase in temporal kinetics of lipidomic and metabolic reprogramming in HF.

Materials and methods: To address this question, we used a permanent coronary ligation mouse model which showed profound metabolic and lipidomic reprogramming in acute HF. Additionally, we defined the lipoxygenase-mediated changes in cardiac pathophysiology in acute and chronic HF. For this, we quantitated systemic metabolic changes and lipidomic profiling in infarcted heart tissue with obvious structural remodeling and cardiac dysfunction progressing from acute to chronic HF in the survival cohort.

Results: After MI, lipoxygenase-derived specialized pro-resolving mediators were quantitated and showed lipoxygenase-deficient mice (12/15LOX$^{-/-}$) biosynthesize epoxyeicosatrienoic acid (EETs; cypoxins) to facilitate cardiac healing. Lipoxygenase-deficient mice reduced diabetes risk biomarker 2-aminoadipic acid with profound alterations of plasma metabolic signaling of hexoses, amino acids, biogenic amines, acylcarnitines, glycerophospholipids, and sphingolipids in acute HF, thereby improved survival.

Conclusion: Specific lipoxygenase deletion alters lipidomic and metabolic signatures, with modified leukocyte profiling that delayed HF progression and improved survival. Future studies are warranted to define the molecular network of lipidome and metabolome in acute and chronic HF patients.

1. Introduction

There is strong evidence that the heart is a metabolically omnivore organ with the high demand for energy in order to circulate nutrients and blood to different parts of the body in a timely manner [1]. Historically, the cardiac metabolism is mainly focused on fatty acids oxidation and the glycolytic pathway ('Randle cycle') that regulate ATP production as the prime energy source of the myocardium [2]. Recent advancement of mass spectrometry-based quantitative measurement of metabolites and integration with molecular and cellular pathways allowed differentiating the quantitative levels of metabolites that demarcates line between physiology and pathology. Recent application of 'ome' techniques and different 'omics' reports suggest that metabolites signature can serve as a biomarker in cardiometabolic health to differentiate physiology and pathology [3–5]. Particularly, the distinction of metabolic remodeling in acute ischemic decompensated heart failure (HF) compared to chronic HF is incomplete due to the complexity of the mammalian metabolic and immune cellular network [6]. Thus, in the presented report, we describe the previously unrecognized and unappreciated metabolite profiles in acute and chronic leukocyte reprogramming as an integral part of molecular mechanisms resulting in HF.

Human and rodent HF syndrome, secondary to myocardial infarction (MI), is an irreversible process that progresses from acute to advanced HF with system-wide impact on the spleen and kidney [7–10]. Human HF is often characterized by an insufficient or imbalance of energy substrates leading to impaired energy dynamics and mechanical HF [6,11]. In response to cardiac injury, there is an accelerated degradation of phospholipids in the ischemic myocardium with a marked increase of ceramide species [6]. As per clinical HF staging guidelines, stage A defines the possible high risk of HF due to hypertension/coronary artery disease without structural and functional abnormality and class D is the end stage of severe HF marked with heart dysfunction, fatigue, and shortness of breath symptoms at rest that require a heart transplant [12,13]. Based on

* Corresponding author at: Department of Medicine, Division of Cardiovascular Disease, The University of Alabama at Birmingham, 703 19th Street South, MC 7755, Birmingham, AL 35294, United States.
E-mail address: ganeshhalade@uab.edu (G.V. Halade).

https://doi.org/10.1016/j.metabol.2019.04.011
0026-0495/

population studies, the diastolic HF epidemic (36%) that ranges from 15.8 to 52.8% is increasing than systolic HF (5.5%) ranges from 3.3 to 9.2% mainly in aging individuals [14]. Thus, measurement of acute and chronic HF-associated systemic metabolic signaling together with advances in nutrigenomic approaches might permit the development of more precise, prognostic, personalized, and preventive measures. Therefore, in this context, the levels of plasma/serum circulating metabolites and lipid species in cardiac tissue are important indicators of physiological and pathological remodeling [5,15].

Lipoxygenase (LOX) are a class of fatty acid-metabolizing enzymes known to govern inflammation by regulating bioactive lipid mediators in cardiac injury [16,17]. Particularly, 12/15LOX (an ortholog of human 12-LOX) is essential for the generation of specialized pro-resolving mediators (SPMs) [18–20], however, genetic deficiencies of 12/15LOX in mice shift lipidomic network towards activation of reparative neutrophils and macrophages to facilitate cardiac healing, survival, and delayed HF [16,17]. Therefore, the present work aims to uncover the role of 12/15LOX in immune cell kinetics, metabolic, and bioactive lipid signatures in acute and progressive advanced HF. Since, metabolomics is developing and is a complex field with at least >6500 metabolites [6], here we precisely selected six specific metabolite classes (hexoses, amino acids, biogenic amines, acylcarnitine, glycerophospholipids, and sphingolipids) comprising 180 metabolites to define the metabolic reprogramming in acute and chronic HF. Collectively, our studies have discovered a novel link of LOX signaling between lipidomic and metabolic signatures in acute and chronic HF syndrome.

2. Methods

2.1. Animal compliance

All surgery protocols involving animals were conducted by the Guide for the Care and Use of Laboratory Animals published by the US National Institutes of Health (revised 2015) and was approved by the Animal Care and Use Committee at the University of Alabama at Birmingham. Detailed methods are provided online as supplementary data.

2.2. Permanent coronary ligation to induce heart failure

To mimic human HF, the MI was induced in wild type (WT; C57BL/6J) and 12/15LOX$^{-/-}$ male mice by surgical ligation of the left anterior descending coronary artery, as described previously [7,21,22]. Mice that died within 24 h after surgery were noted as peri-operative mortality (4%) similar in both groups and were added in the survival outcome. As shown in the study design (Fig. 1A), with an overlap on survival curve, a total of three mice cohorts were used to define lipidomic and metabolic reprogramming in acute and chronic HF. The first cohort was used for left ventricle (LV) lipidomics and histological analyses. The second cohort was used for metabolites quantitation and leukocyte profiling in acute and chronic HF. The third cohort was monitored for survival. For all three cohorts, acute HF was confirmed on day 1 after MI surgery using echocardiography and mice with fractional <10%

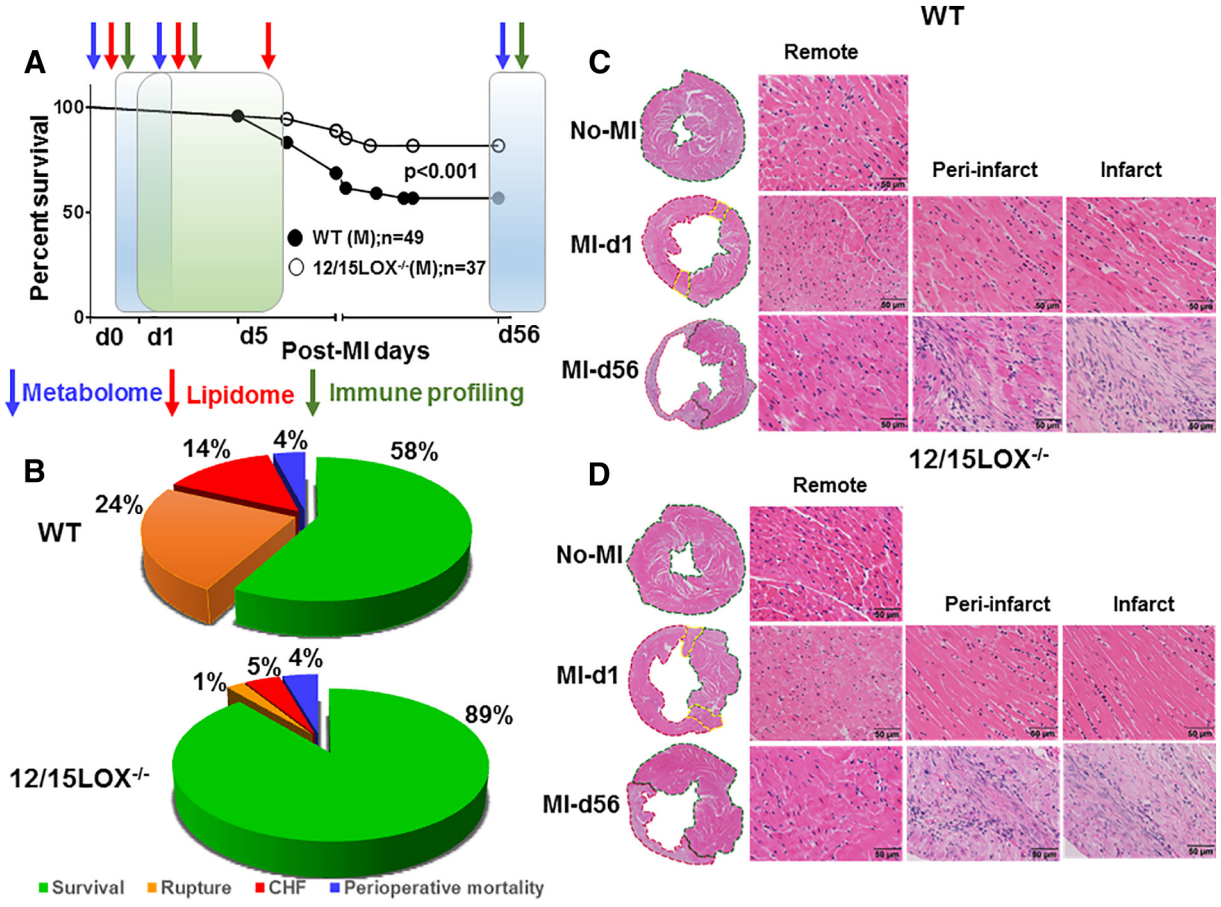

Fig. 1. (A) Study design superimposed with different time points selected for metabolome, lipidome, and leukocyte profiling, and survival rates post-MI in WT and 12/15LOX$^{-/-}$ mice analyzed by log-lank test. *$p < 0.01$ vs. WT (male, $n = 49$), 12/15LOX$^{-/-}$ (male, $n = 37$). The overlapping blue-green shade of survival curve indicate the time point of profound inflammatory response while green shade explains the resolution of inflammation post-MI. (B) Pie chart representing overall percentage of peri-operative mortality, survival, congestive heart failure (CHF), and ruptures post-MI in WT and 12/15LOX$^{-/-}$ mice. (C–D) Representative hematoxylin and eosin stained LV images from d0 naïve control (no-MI), MI-d1 suggestive of acute HF, and MI-d56 indicative of chronic HF of WT (C) and 12/15LOX$^{-/-}$ mice (D). Representative images of remote (left), peri-infarct (middle), and infarct area (right) with a magnification of 40× and accompanying 1.25× images (far left; dotted green line represents remote area, dotted red line represents infarcted area and dotted yellow line represents area of risk); scale bar = 50 μm.

were included in the study. Mice with fractional shortening above 10% were excluded from the present study in order to define precise and long-term survival and leukocyte profiling in acute and chronic HF. Heart functional data was reported from the survival cohort. In order to avoid the female mice menstrual cycle-related leukocyte activity during the acute and chronic HF, male mice are used in the presented study to define the HF immune cell profiling [23].

2.3. Necropsy

Mice were anesthetized with 2% isoflurane in an oxygen mix and injected with 4 IU/g heparin, as previously reported [7]. The lungs, LV, right ventricle (RV), and spleen were separated and weighed individually. Blood was collected and plasma was used for metabolomics analyses using mass spectrometry. LV-middle sections were fixed in 10% zinc formalin for immunohistochemistry and LV apex was used for lipidomics analyses. The rest of the LV was snap frozen for molecular analysis, as described previously [7].

2.4. Transthoracic echocardiography

Vevo 3100 (VisualSonics Inc., Canada) in vivo imaging system was used to perform echocardiography equipped with probes of up to 40 MHz and a resolution of 30 μm. Mice were anesthetized with 1.5–2% isoflurane in an oxygen mix. Heart rate (>400 beats per min), respiratory rate, and body temperature (35–37 °C) were continuously monitored throughout the procedure to ensure an adequate depth of anesthesia. Echocardiographic speckle tracking-based strain measures of myocardial deformation were obtained from two-dimension gray-scale echocardiography images acquired from long- and short-axis views [7,18].

2.5. LV hematoxylin and eosin staining

For histological measurements, LV mid-cavity longitudinal sections were embedded in paraffin and sectioned. Sections were stained with hematoxylin and eosin. LV images were acquired for each mouse using a microscope (BX43) with an attached camera (Olympus DP73). A total of five to six images were acquired per mouse per group [7].

2.6. LV collagen staining using picrosirius red

Picrosirius red (PSR) staining was used to measure the collagen density in the paraffin-embedded LV-mid cavity sections of all experimental mice. PSR stained sections were imaged with precise differentiation of remote, peri-infarct, and infarct area as described previously [7].

2.7. Targeted lipidomics using mass spectrometry

After necropsy, the LV tissues from naïve controls d0, MI-d1, and MI-d5 (~15 mg) were taken from WT and 12/15LOX$^{-/-}$ mice and homogenized in 1:9 ratio with 1× PBS (pH 7.4) and centrifuged at 10,000 rpm for 5 min at 4 °C. The supernatant was collected, and protein was measured using Bradford kit (Biorad Inc.). The samples were further extracted using solid phased extraction methodology for targeted lipidomics using liquid chromatography–tandem mass spectrometry as described previously [24].

2.8. Metabolites analysis using mass spectrometry

Samples were prepared using the AbsoluteIDQ® p180 kit (Biocrates Innsbruck, Austria) in strict accordance with their detailed protocol. After the addition of 10 μL of the supplied internal standard solution to each well of the 96-well extraction plate, 10 μL of each study sample were added to the appropriate wells. The plate was then dried under a gentle stream of nitrogen. The samples were derivatized with phenyl isothiocyanate then eluted with 5 mM ammonium acetate in methanol. Samples were diluted with either water for the UPLC analysis (4:1) or running solvent (a proprietary mixture provided by Biocrates) for flow injection analysis (20:1). The detailed protocol is provided in the Supplementary metabolic methodology. The Absolute*IDQ*® p180 quantitative kit (BIOCRATES Life Sciences, Austria) targets over 180 metabolites from five analyte groups: acylcarnitines, amino acids, biogenic amines, glycerophospholipids, and sphingolipids. The p180 kit includes all requisite calibration standards, internal standards, and QC samples. The use of these standards according to the detailed analysis protocol which was validated in Biocrates' lab in Austria assures assay harmonization and standardization within a project, across projects, and laboratories. Selective analyte detection is accomplished by use of a triple quadrupole tandem mass spectrometer operated in Multiple Reaction Monitoring (MRM) mode in which specific precursor to product ion transitions are measured for every analyte, and stable isotope labeled internal standard [25]. There are two separate tandem mass spectrometric analyses of each sample. For the analysis of acylcarnitines, glycerophospholipids, and sphingolipids samples are introduced using a Flow Injection Analysis method (FIA-MS/MS, Supplementary metabolic methodology). Analysis of amino acids and biogenic amines are performed by a UHPLC (ultra-high pressure liquid chromatography) tandem MS method using a reversed phase analytical column for analyte separation (LC-MS/MS, Supplementary metabolic analyses methodology) [15,25–27].

2.9. LV flow cytometry in acute and chronic HF

After necropsy, the LV mononuclear cells were isolated from acute HF (MI-d1), and chronic HF (MI-d56) WT and 12/15 LOX$^{-/-}$ mice as described in previous reports [17]. The flow cytometry and analyses was performed as previously described [17]. The detailed leukocyte markers strategies are provided in Supplementary Fig. 1.

2.10. Statistical analysis

Data are expressed as mean per group and standard error of the mean (SEM). Statistical analyses were performed using GraphPad Prism 5. Analysis of variance (ANOVA), followed by Newman-Keuls post hoc test, was performed for multiple comparisons of post-MI-d1, d5, or d56 compared to d0 naïve control. Kaplan-Meier and the log-rank test were used for survival analyses. For comparison of two groups, Student's *t*-test (unpaired) was applied and $p < 0.05$ was considered as statistically significant.

3. Results

3.1. Coronary ligation surgery induced obvious structural, fibrotic, and pathological remodeling with improved survival in 12/15LOX$^{-/-}$ mice compared to WT controls

In response to occlusion of the left anterior descending coronary artery, the mice developed acute decompensated HF within 24 h that continued to advance chronic HF [7]. Post-MI survival was higher in 12/15LOX$^{-/-}$ mice compared with WT 89% vs. 58% (Fig. 1A). As the impact of coronary ligation, mice developed intense leukocyte infiltration and marked with ventricle rupture in the inflammation-resolution phase of cardiac healing. 12/15LOX-deficient mice were more resistant to rupture compared with WT (1% vs. 24%; Fig. 1B). The left ventricle myocardium of d0 naïve control mice shows elongated cardiomyocytes with centrally located nuclei and intercalated disks indicating a healthy heart (Fig. 1C-D, top panel). After MI, the infarcted tissue showed large scale apoptosis suggestive of myofibrillar lysis, contraction bands, and coagulative necrosis in the ventricular myocardium with signs of cardiac injury and beginning of wall-thinning in acute HF (Fig. 1C-D, middle panel). Prolonged ischemia resulted in irreversible chronic HF marked with reactive fibrosis, and

high amount of collagenous tissue intersects between cardiomyocytes (Fig. 1C-D, bottom panel). The wall-thinning was evident by hematoxylin, and eosin stained LV myocardium of WT and 12/15LOX$^{-/-}$ mice particularly in chronic HF, and fibrosis was validated by PSR staining that was noticed particularly in chronic HF. After cardiac injury in both genotypes, fibrosis was absent in acute HF (day 1); however, patchy fibrosis was observed in the peri-infarct area, and dense fibrotic remodeling was obvious in the infarcted area of chronic HF mice (day 56).

Echocardiography parameters were assessed to determine the impact of 12/15LOX deletion on LV function and remodeling in the post-MI setting. Temporal echocardiography data from survival cohort (Supplementary Table 1) reveal decreased dimensions of LV parameters such as end-systolic dimension (ESD) and end-diastolic dimension (EDD) at d1 and d56 post-MI thereby improved fractional shortening in 12/15LOX$^{-/-}$ mice compared with WT, indicative of improved LV function post-MI. Although both WT, 12/15LOX$^{-/-}$ deficient mice showed longitudinal segmental dyssynchronicity by post-MI-D1 as shown (Fig. 2A–B, middle and bottom panel) in the synchronicity images, the anterior base (blue line) and posterior base (green line) compensated the LV function because of anterolateral infarction in post MI-d1 in WT mice where as its compensated by entire LV except anterior base in 12/15LOX$^{-/-}$ mice, this can also visually noticed in long axis B-mode speckle tracking images. Also, enhanced longitudinal strain was noticed in 12/15LOX$^{-/-}$ deleted mice compared to WT mice in both acute and chronic HF. PSR staining was performed to evaluate the mature scar formation in chronic HF in both WT and 12/15LOX$^{-/-}$ mice. Thus, deletion of 12/15LOX in mice had limited dilatation with minimal impact on fibrosis since the infarcted myocardium showed similar patchy fibrosis in the peri-infarct region and compact dense fibrosis in the infarcted area (Fig. 2C-D, middle and bottom panel) compared to WT mice mainly in chronic HF that revealed the intense remodeling in advanced HF after successful coronary ligation.

3.2. 12/15LOX deletion programs metabolic substrate shunting for biosynthesis of bioactive lipid mediators in acute HF post-MI

After cardiac injury, activated LOXs (−5, −12, and −15) are essential for biosynthesis of SPMs [18], as expected WT mice biosynthesized resolvin (RvD)1, RvD3–5, protectin D1, aspirin-triggered RvD1, lipoxin A_4, lipoxin B_4, and aspirin-triggered lipoxin A_4 in the infarcted heart compared with 12/15LOX$^{-/-}$ mice, suggestive of an impaired enzymatic conversion of essential fatty acids to bioactive lipid mediators (Fig. 3A–B). At homeostatic equilibrium, the SPMs were undetected or in insignificant traces in the myocardium; in response to cardiac ischemic injury, the SPMs are biosynthesized within 24 h and reached to day (d) 0 naïve control level by d5 post-MI. In contrast, 12/15LOX$^{-/-}$ mice showed impaired SPMs biosynthesis but increased cytochrome P450 epoxygenase-mediated three epoxyeicosatrienoic acids (cypoxins) suggestive of essential fatty acids substrate shunting during specific 12/15LOX deficiency (Fig. 3C–D). Infarcted LV of 12/15LOX deficient mice increased cypoxins specifically epoxyeicosatrienoic acid (5,6-EET; 13 ± 0.8 ng/50 mg vs. 10 ± 1 ng/50 mg), (11,12-EET; 170 ± 21 ng/50 mg vs. 94 ± 5 ng/50 mg), (14,15-EETs; 93 ± 8 ng/50 mg vs. 52 ± 3 ng/50 mg) particularly at d1 post-MI in acute HF (Fig. 3E–G) and remained elevated at d5 post-MI, suggestive of long-term metabolic shunting. Thus, in 12/15LOX$^{-/-}$ mice cytochrome P450 epoxygenase cypoxins that regulate cardiac healing despite the impaired biosynthesis of SPMs suggestive of profound metabolic enzyme-substrate shunting in mice post-MI.

3.3. Monogenic 12/15LOX deletion in mice reprogrammed metabolic signaling towards cardioprotection

While in naïve controls (d0; no-MI) there is homeostatic equilibrium, 12/15LOX$^{-/-}$ mice exhibited altered metabolic signaling.

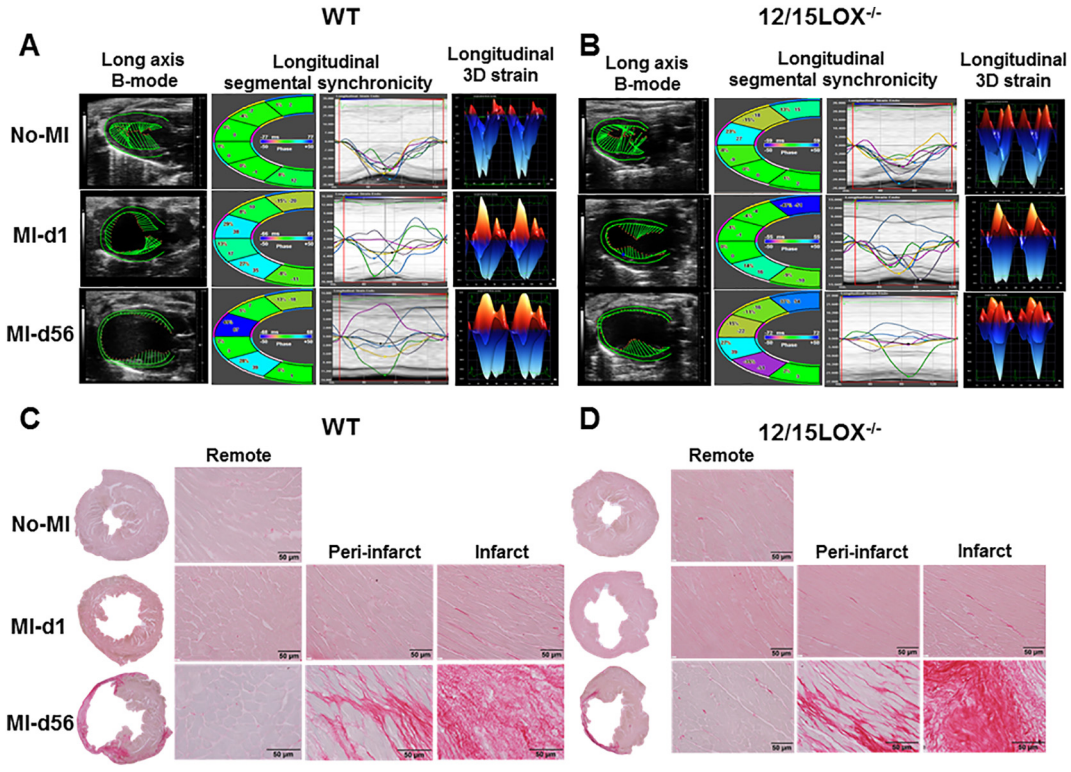

Fig. 2. (A–B) Speckle tracking-based representative echocardiography images of LV in long axis B-mode (left), longitudinal segmental synchronicity (middle panel) and longitudinal 3D strain (right) in naïve controls (no-MI) and compared with acute decompensated HF (MI-d1) and chronic HF (MI-d56) in (A) WT and (B) 12/15LOX$^{-/-}$ mice. (C–D) Representative picrosirius red stained LV images in naïve controls (no-MI) compared with acute HF (MI-d1) and chronic HF (MI-d56) of WT (C) and 12/15LOX$^{-/-}$ mice (D). Picro-sirius red stained representative LV images of remote (left), peri-infarct (middle), and infarct area (right) with a magnification of 40× and accompanying 1.25× images (far left); scale bar = 50 μm.

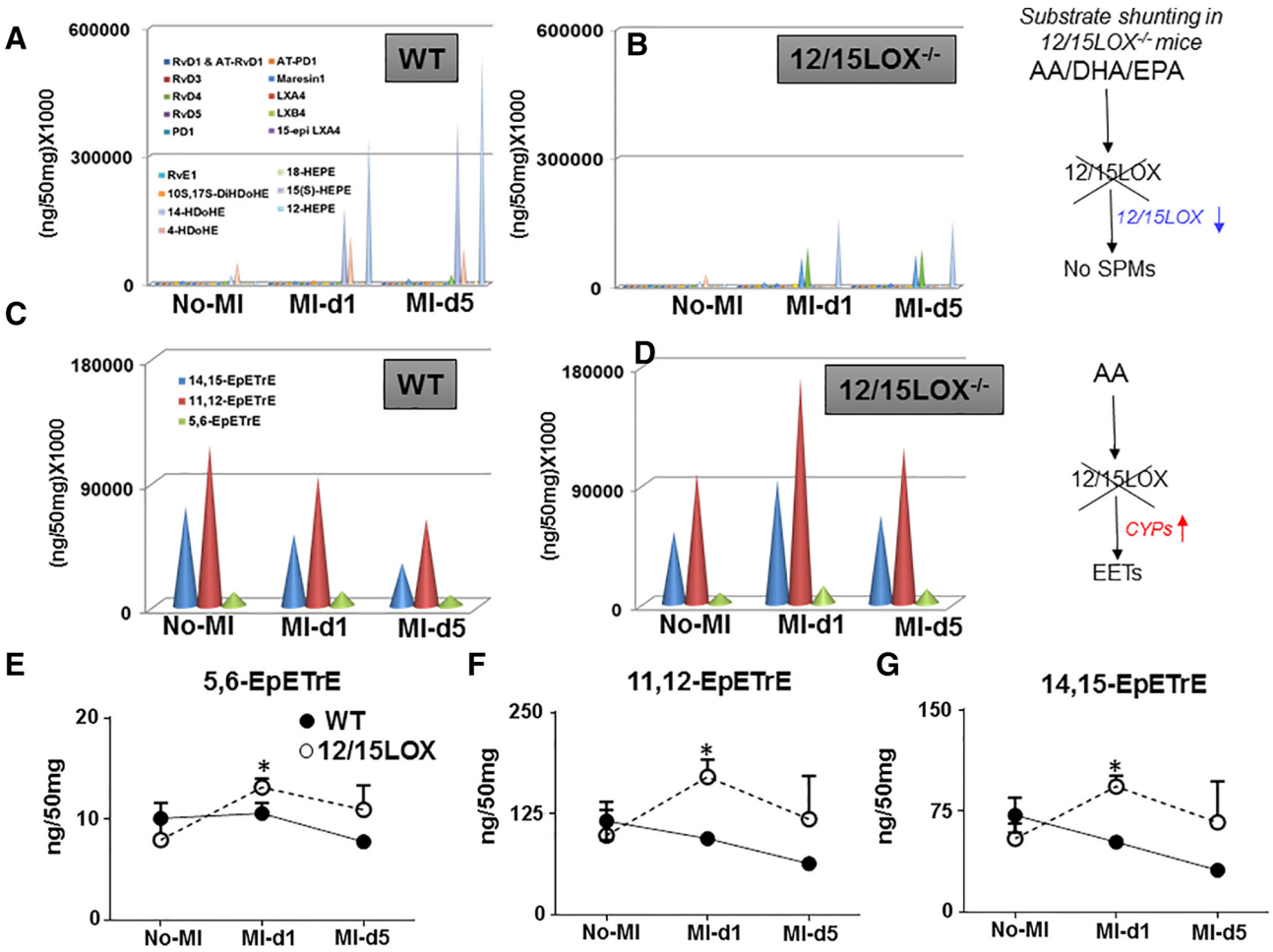

Fig. 3. Quantitative representation of lipidome comprised of specialized pro-resolving mediators (SPMs) in ng/50 mg × 1000 of LV using LC-MS in naïve controls and at d1 and d5 post-MI in (A) WT and (B) 12/15LOX$^{-/-}$ mice. Quantitative representation of lipidome using cone graphs comprised of AA lipid mediators in LV using LC-MS-MS in naïve controls and at d1 and d5-post-MI in (C) WT and (D) 12/15LOX$^{-/-}$ mice. (E) Line graphs of 5,6-EpETrE (EET) in ng/50 mg of LV at naïve controls d0, d1, and d5-post-MI in WT and 12/15LOX$^{-/-}$ mice. (F) Line graph of 11,12-EpETrE (EET) in ng/50 mg of LV at d0, d1, and d5-post-MI in WT and 12/15LOX$^{-/-}$ mice. (G) Line graph of 14,15-EpETrE (EET) in ng/50 mg of LV at d0, d1 and d5-post-MI in WT and 12/15LOX$^{-/-}$ mice. *$p < 0.05$ compared with WT at respective time point.

Monogenic deletion of 12/15LOX led to an increase of five amino acids (red), arginine, citrulline, glutamine, lysine, and spermidine, while two aromatic amino acids (blue), tryptophan and phenylalanine, were down regulated (Fig. 4A–F). The concentration of arginine (134 ± 5 μM vs. 105 ± 9 μM; $p = 0.016$) was observed to be highest in 12/15LOX$^{-/-}$ mice, while diabetes risk marker 2-aminoadipic acid (1.3 ± 0.07 μM vs. 8.1 ± 1 μM; $p < 0.0001$) was significantly lowered compared with WT (Fig. 4B and F, Supplementary Table 2). Since aromatic amino acids are not metabolized in the heart, the decrease of tryptophan and phenylalanine in 12/15LOX$^{-/-}$ mice could be a consequence of fat-metabolizing enzyme deficiency leading to diversified metabolic signaling. Thus, 12/15LOX deletion reprogrammed metabolic signatures towards the cardioprotective side with reduced levels of diabetes risk marker and an increase in levels of metabolites that are associated with cardiac health.

3.4. Ischemic injury in acute decompensated HF marked with profound metabolic signatures

To examine whether monogenic deletion of 12/15LOX in acute HF influenced novel aspects of metabolic signaling and cardiac healing, we quantitated plasma amino acid/acylcarnitine profiling in 12/15LOX$^{-/-}$ versus WT aged-matched control mice post-MI d1. Among 180 metabolites analyzed, 12 amino acids, 1 acylcarnitine, 17 glycerophospholipids, and 6 sphingolipids were significantly elevated in 12/15LOX$^{-/-}$ mice compared with WT at post-MI-d1 (Supplementary Fig. 2 - heat map). However, 4 amino acids, 9 acylcarnitine, and 15 glycerophospholipids were significantly decreased in 12/15LOX$^{-/-}$ mice compared with WT mice. The quantitative tandem mass spectrometry-based analyses of plasma from 12/15LOX$^{-/-}$ mice revealed higher amounts of arginine, ornithine, as well as the polyamines spermidine and spermine with no change in citrulline in the acute HF (Fig. 5A–D; Supplementary Fig. 3). Interestingly, 12/15LOX$^{-/-}$ plasma displayed elevated levels of methionine, which is a sulfur-containing amino acid and enters the body through dietary proteins, is used in forming proteins in the body, and is the precursor (through the methionine cycle) of the sulfur-containing amino acids homocysteine, cysteine, and taurine, which remain unchanged (Fig. 5F). The Krebs cycle intermediates, such as glutamate and phenylalanine, were decreased, but asparagine was increased (Fig. 5G). Quantitative analyses revealed that 12/15LOX deletion increased alanine (940 ± 90 μM vs. 394 ± 86 μM; $p < 0.0043$), arginine (143 ± 8 μM vs. 93 ± 11 μM; $p < 0.0039$), lysine (447 ± 15 μM vs. 279 ± 30 μM; $p < 0.0006$) compared with WT. 12/15LOX deletion led to increase levels of lysine but its metabolic product 2-aminoadipic acid was significantly down regulated (1.5 ± 0.1 μM vs. 8 ± 2 μM; $p < 0.0001$) and phenylalanine (78 ± 4 μM vs. 100 ± 7 μM; $p < 0.0249$) compared with WT (Fig. 5B–F). The analyses of the glycerophospholipids displayed a combined impact: 12/15LOX deletion displayed a decrease in lysoPC a (C16:1), PC aa C32:1, PC aa C34:3, PC aa C34:4, PC aa C36:0, PC aa C36:1, PC aa C36:5, PC aa C36:6, PC aa C38:5, PC aa C38:6, PC ae C38:0, PC ae C40:1, PC ae C40:2, PC ae C42:2,

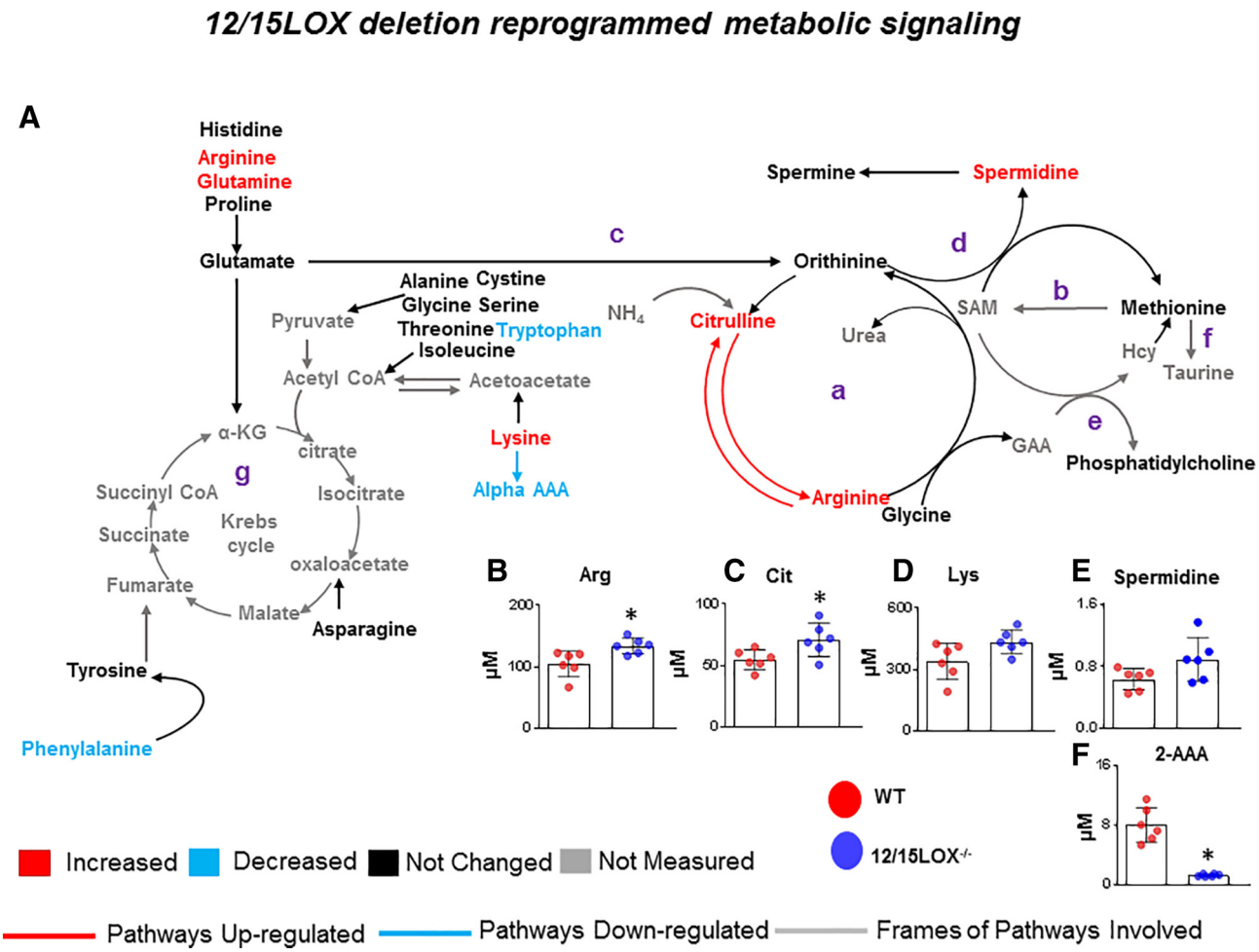

Fig. 4. (A) 12/15LOX deletion reprogrammed metabolic signatures in the following metabolic network: (a) urea cycle, (b) MTA/methionine cycle, (c) ornithine-proline-glutamate, (d) polyamine synthesis, (e) methylation (phosphatidylcholine), (f) transsulfuration (taurine) and (g) Kreb's cycle. Metabolites marked in red, blue, black, and gray indicate the abundance of metabolite species which increased or decreased significantly, remained unchanged, or were not measured, respectively. α-KG, alpha-ketoglutarate; BH4, tetrahydrobiopterin; GAA, guanidinoacetate; Hcy, homocysteine; MTA, 5-methylthioadenosine; NO, nitric oxide; PE, phosphatidylethanolamine; SAM, S-adenosylmethionine. (B) Arginine, (C), citrulline, (D) lysine, (E) spermidine were significantly increased, whereas (F) 2-AAA was decreased due to 12/15LOX deletion compared with WT (*$p < 0.05$ compared with WT).

and PC ae C42:3, while glycerophospholipids lysoPC a (C18), PC aa C40:2, PC aa C40:4, PC aa C42:0, PC aa C42:1, PC aa C42:2, PC aa C42:4, PC ae C34:2, PC ae C34:3, PC ae C36:4, PC ae C36:5, PC ae C38:1, PC ae C38:2, PC ae C38:4, PC ae C38:5, PC ae C40:4, and PC ae C44:6 were increased in 12/15LOX$^{-/-}$ mice (Supplementary Table 3). Further, analyses of sphingolipids displayed elevated levels of SM(OH)C14:1, SM C16:0, SM C16:1, SM C24:0, SM C24:1, and SM C26:0 in 12/15LOX$^{-/-}$ mice compared with WT (Supplementary Table 3). In comparison to WT, deletion of 12/15LOX displayed comprehensive and profound metabolic reprogramming particularly in metabolites of the urea cycle and sphingolipids in acute decompensated HF.

3.5. Metabolic remodeling in chronic HF

In chronic HF, the glycerophospholipids were significantly dysregulated after deletion of 12/15LOX (Supplementary Table 4), however many metabolites remained unchanged. Compared with WT mice, circulating metabolites related to ADMA, histamine, and putrescine, (Fig. 6A), Though, spermidine was relatively elevated before MI in 12/15LOX$^{-/-}$ mice and significantly increased in acute HF but did not observed significant changes in chronic HF compared to WT mice (Fig. 6B-C, Supplementary Table 4). 2-Aminoadipic acid, an aromatic amino acid, (1.2 ± 0.1 μM vs. 6.4 ± 0.5 μM; $p < 0.0001$) was significantly lower in 12/15LOX$^{-/-}$ mice in chronic HF at post-MI d56 compared with WT (Fig. 6D). Like advanced HF patients metabolic signatures [15], in 12/15LOX null mice 63 glycerophospholipids (Supplementary Table 4) and 3 sphingolipids (SM(OH) C24:1, SM C20:2, SM C26:0) were significantly downregulated, while the putrescine and spermidine were upregulated compared with WT mice. Thus, HF metabolic reprogramming in mice is comparative related to major metabolites in acute HF and contrasting to few metabolites in chronic HF syndrome.

3.6. Immune cell profiling in acute and chronic HF

The diverse microenvironment of individual metabolites is critical for defining leukocyte phenotypes and function. We further evaluated acute early biphasic and chronic immune response in WT and 12/15LOX$^{-/-}$ mice by flow cytometry. Based on CD206 and Ly6C$^{hi/lo}$ expression patterns in acute HF (post-MI-d1), 12/15LOX$^{-/-}$ mice had a higher population of Ly6C^{lo} compared to WT in LV. The expression analysis of Ly6C^{lo}/CD206^{+} by histogram revealed that 12/15LOX$^{-/-}$ mice displayed higher expression compared with WT mice (Fig. 7A–B). 12/15LOX$^{-/-}$ mice showed a higher percentage (125 ± 25 cells/mg infarct LV; $p < 0.05$) of reparative macrophages (Ly6C^{lo}/CD206^{+}) compared to WT in acute HF (Fig. 7C). Tregs constitute a subset of CD4^{+} T cells are known to regulate immune inflammatory function; we quantitated Treg kinetics in acute and chronic HF syndrome. Treg cells were sorted based on CD4^{+}/CD127^{-}/CD25^{+}/Foxp3^{+} expression. In acute HF, Tregs

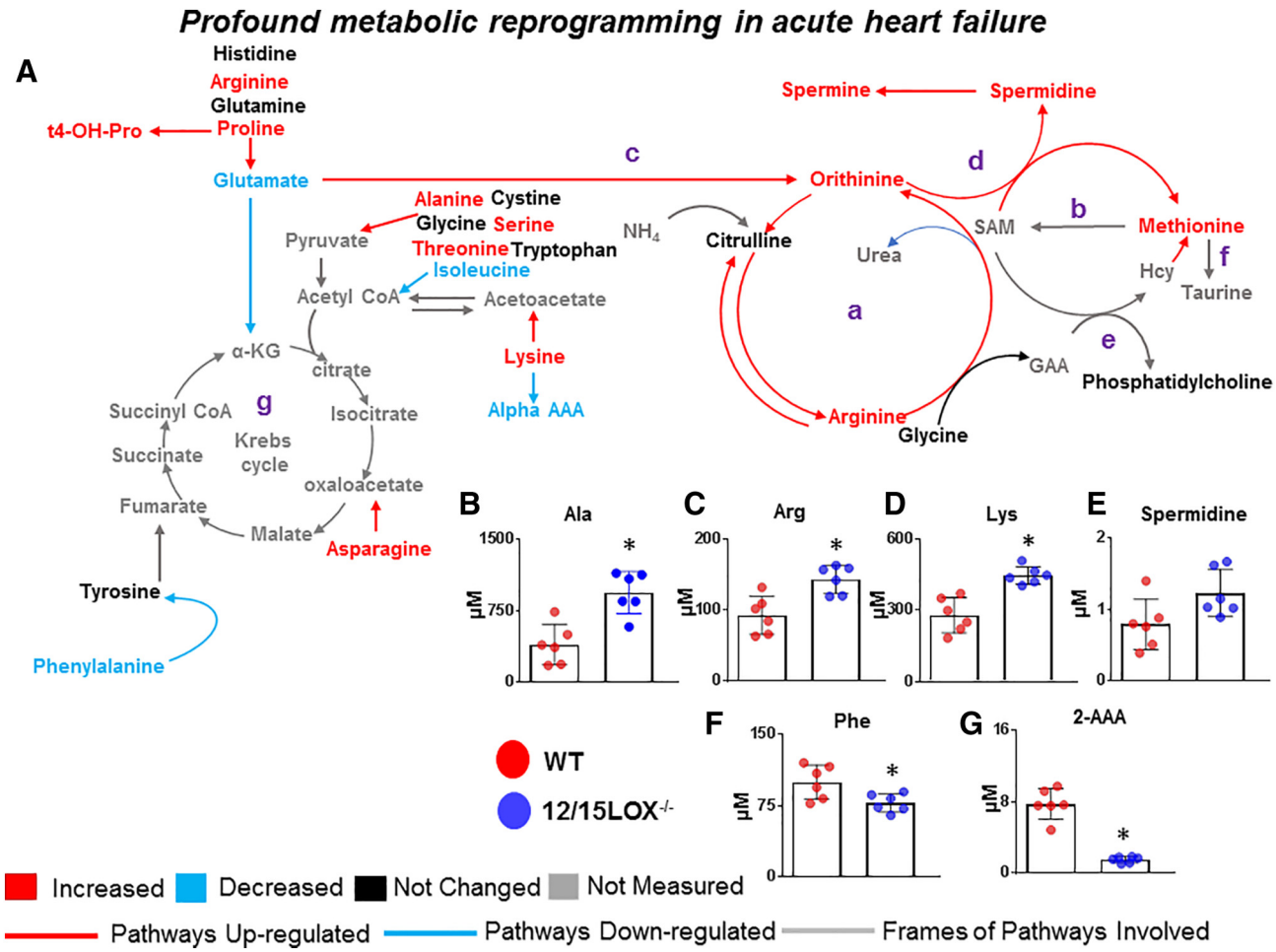

Fig. 5. (A) Cardiac injury induced profound metabolic reprogramming in acute HF in the following metabolic pathways: (a) urea cycle, (b) MTA/methionine cycle, (c) ornithine-proline-glutamate, (d) polyamine synthesis, (e) methylation (phosphatidylcholine), (f) transsulfuration (taurine), and (g) Kreb's cycle. Metabolites marked in red, blue, black, and gray indicate the abundance of metabolites species which significantly increased, decreased, remained unchanged, or were not measured, respectively. α-KG, alpha-ketoglutarate; BH4, tetrahydrobiopterin; GAA, guanidinoacetate; Hcy, homocysteine; MTA, 5-methylthioadenosine; NO, nitric oxide; PE, phosphatidylethanolamine; SAM, S-adenosylmethionine. Precise quantitative levels in μM that were (B) Alanine, (C) arginine, (D) lysine, (E) spermidine were increased, whereas (F) phenylalanine and (G) 2-AAA were decreased due to 12/15LOX deletion compared with WT (*$p < 0.05$ compared with WT).

were low, while 12/15LOX$^{-/-}$ mice displayed higher number of CD4$^+$/CD127$^-$/CD25+/Foxp3$^+$ population in acute HF (0.07 ± 0.01%) compared with WT which displayed 0.003 ± 0.001% population (Fig. 7D). Foxp3 expression was higher in 12/15LOX$^{-/-}$ mice compared with WT (Fig. 7E). Evaluation of total cell density revealed 4 ± 0.5 cells/mg infarct LV in 12/15LOX$^{-/-}$ compared with WT which showed 2 ± 1 cells/mg infarct LV (Fig. 7F). In chronic HF (post-MI-d56), innate immune response completely subsided. In line with previous results regarding innate immune cells kinetics, macrophages (F4/80$^+$/Ly6C$^+$) were decreased in chronic HF (Fig. 7G). Of note, 12/15LOX$^{-/-}$ mice displayed higher expression of reparative Ly6C^{lo}/CD206$^+$ macrophages compared with WT mice (Fig. 7G). We noted 11 ± 1 cells/mg infarct LV Ly6C^{lo}/CD206$^+$ macrophages compared with WT mice which displayed 7 ± 1 cells/mg infarct LV in chronic HF (Fig. 7H). Quantitation of Treg cells in the infarcted LV in chronic HF settings revealed an increase in CD4$^+$/Foxp3$^+$ cells at d56 post-MI. 12/15LOX$^{-/-}$ mice displayed consistent increase in the CD4$^+$/CD127$^-$/CD25$^+$/Foxp3$^+$ population (1 ± 0.02%) compared with WT (0.7 ± 0.01%) (Fig. 7J). Compared with WT mice, 12/15LOX$^{-/-}$ displayed higher Foxp3 expression (Fig. 7K). 12/15LOX$^{-/-}$ mice showed 7 ± 1 cells/mg in the infarcted LV CD4$^+$/Foxp3$^+$ T cells compared to WT which displayed 4 ± 1; cells/mg in LV infarct during chronic HF (Fig. 7L). Thus, cardioprotective plasma metabolome with reduced levels of 2-aminoadipic acid and cypoxins-enriched lipidome in 12/15LOX null mice reprogrammed leukocyte profiling in acute cardiac injury and thereby improved LV function and survival in chronic HF.

4. Discussion

Derangement of the immune metabolism may contribute to the development of HF syndrome [4,6,15]. Physiologically, the mammalian heart is known to be omnivorous and flexible to utilize different lipidomic and metabolic substrates depending on the availability intertwined with leukocyte trafficking, however the quantitative lipidomic and metabolic flux in cardiac healing from acute to chronic HF is unclear [28]. In mice, deletion of leukocyte responsive 12/15LOX enzyme altered homeostatic equilibria and lowered levels of diabetes biomarker α-aminoadipic acid with profound infarcted heart lipidomic remodeling in the acute HF, thereby delayed chronic HF. Deficiency of 12/15LOX in mice promoted cardiac healing and survival with: 1) marked decreased of 2-aminoadipic acid metabolite in plasma; 2) increased bioactive mediators cypoxins in the infarcted heart in compensation with LOX-derived SPMs; and 3) profound changes in leukocytes trafficking and metabolites signaling of hexoses, amino acids, biogenic amines, acylcarnitines, glycerophospholipids, and sphingolipids in

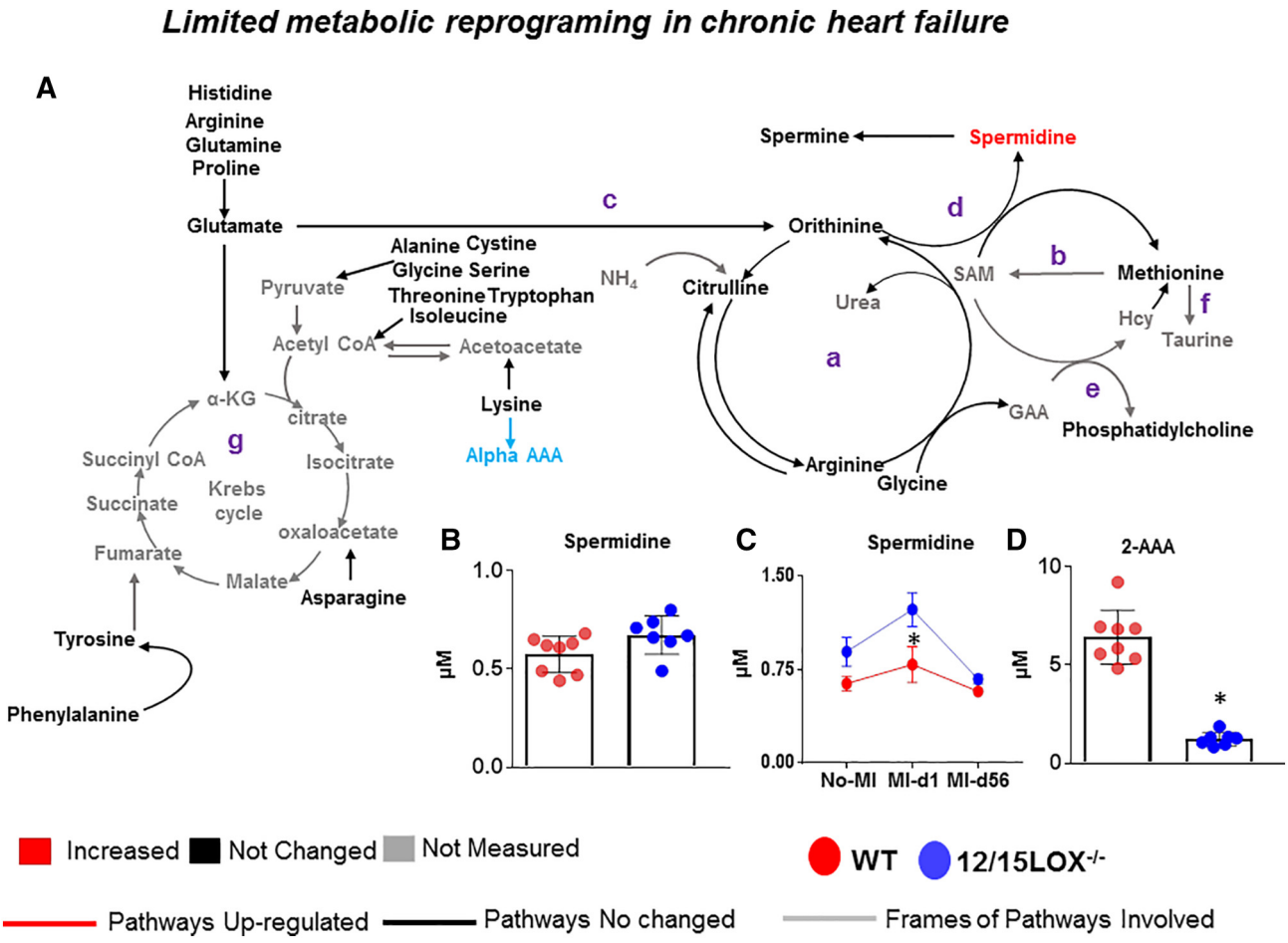

Fig. 6. (A) Limited metabolic reprogramming in chronic HF with 12/15LOX deletion in mice that upregulated (d) ornithine-proline-glutamate cycle with profound homeostasis in (a) urea cycle, (b) MTA/methionine cycle, (c) ornithine-proline-glutamate, (d) polyamine synthesis, (e) methylation (phosphatidylcholine), (f) transsulfuration (taurine), and (g) Kreb's cycle in chronic HF condition. (B) Spermidine was increased in 12/15LOX$^{-/-}$ mice compared with WT, (C) Spermidine dynamics at d0 (no-MI) compared to MI-d1 acute HF and MI-d56 chronic HF post-MI, (*$p < 0.05$ compared with WT-d0) and (D) 2-AAA was decreased in 12/15LOX$^{-/-}$ mice compared with WT (*$p < 0.05$ compared with WT).

acute HF with obvious structural and fibrotic remodeling in chronic HF syndrome.

4.1. Fat remodels into bioactive lipid mediators in acute HF

Fat intake is essential for total health; however, excessive fat intake is the primary cause for obesity and inflammation [29–31]. At homeostatic level, the heart relies to 60–90% on fatty acids oxidation for energy production [28]; in response to coronary ligation injury, immune responsive LOX-enriched splenic leukocytes facilitate biosynthesis of SPMs such as D- and E-series resolvins, maresins, protectins, lipoxins, and aspirin-triggered resolvins in cardiac healing and other models of inflammation-resolution physiology [18,32–34]. In contrast, deletion of fatty acid metabolizing enzyme 12/15LOX in mice facilitated biosynthesis of cypoxins in the spleen and heart to operate resolution of inflammation and cardiac repair of the infarcted heart [16,17]. Human studies clearly indicate that asplenic patients increase the risk of thrombocytosis, hypercoagulability, and possible events of fatal myocardial ischemia [35]. Splenic leukocyte-derived bioactive lipids, such as SPMs and cypoxins, are immune responsive molecules with individual variation in potency and that are biosynthesized in response to injury, infection, and stress [20,36,37]. Therefore, limited abundance in naïve controls suggested that cardiac injury operates based on the cardinal signals with leukocyte infiltration that programs biosynthesis of lipid mediators in the spleen and at the site of injury in acute HF [18]. Presented reports validated that innate immune response overlaps with the resolution phase in cardiac healing with the biosynthesis of SPMs in acute HF [18]. Furthermore, deficiency of 12/15LOX activates cytochrome P450 epoxygenase network that generates cypoxins molecules in lieu of SPMs.

4.2. Fat processing 12/15LOX enzyme defines the lipidome and metabolome

Immune responsive 12/15LOX deficiency in mice altered the homeostatic equilibria with significantly reduced levels of plasma 2-aminoadipic acid which is an established biomarker for diabetes [38]. At the physiological level, 2-aminoadipic acid intake regulates glucose homeostasis and in vitro exposure to islets facilitate insulin secretion in murine and human islets [38]. Therefore, the 12/15LOX deficient mice may be resistant to diabetes, obesity, and metabolic syndrome with marked alteration of leukocyte profile and lipid mediators [39]. At naïve homeostatic level, the cardiac function is indifferent in WT and 12/15LOX deficient mice; however, the metabolites such as arginine, citrulline, lysine, and spermidine were increased suggestive of profound metabolic signaling in response to monogenic alteration in mice. In contrast, a decrease in aromatic amino acids, like tryptophan and phenylalanine, was detected, which is newly discovered and validated as a targeted metabolite in C stage HF patients [15].

Targeted metabolomics analysis in acute HF validated a 'metabolic signatures storm,' with amplified amino acid signals and substrates such as glutamate or tyrosine entering Krebs cycle suggestive of an immune-response directed metabolic reprogramming [40]. In acute decompensated pre-HF, the metabolic signatures are intense like 'cytokine storm' with a marked increase of alanine, arginine, lysine,

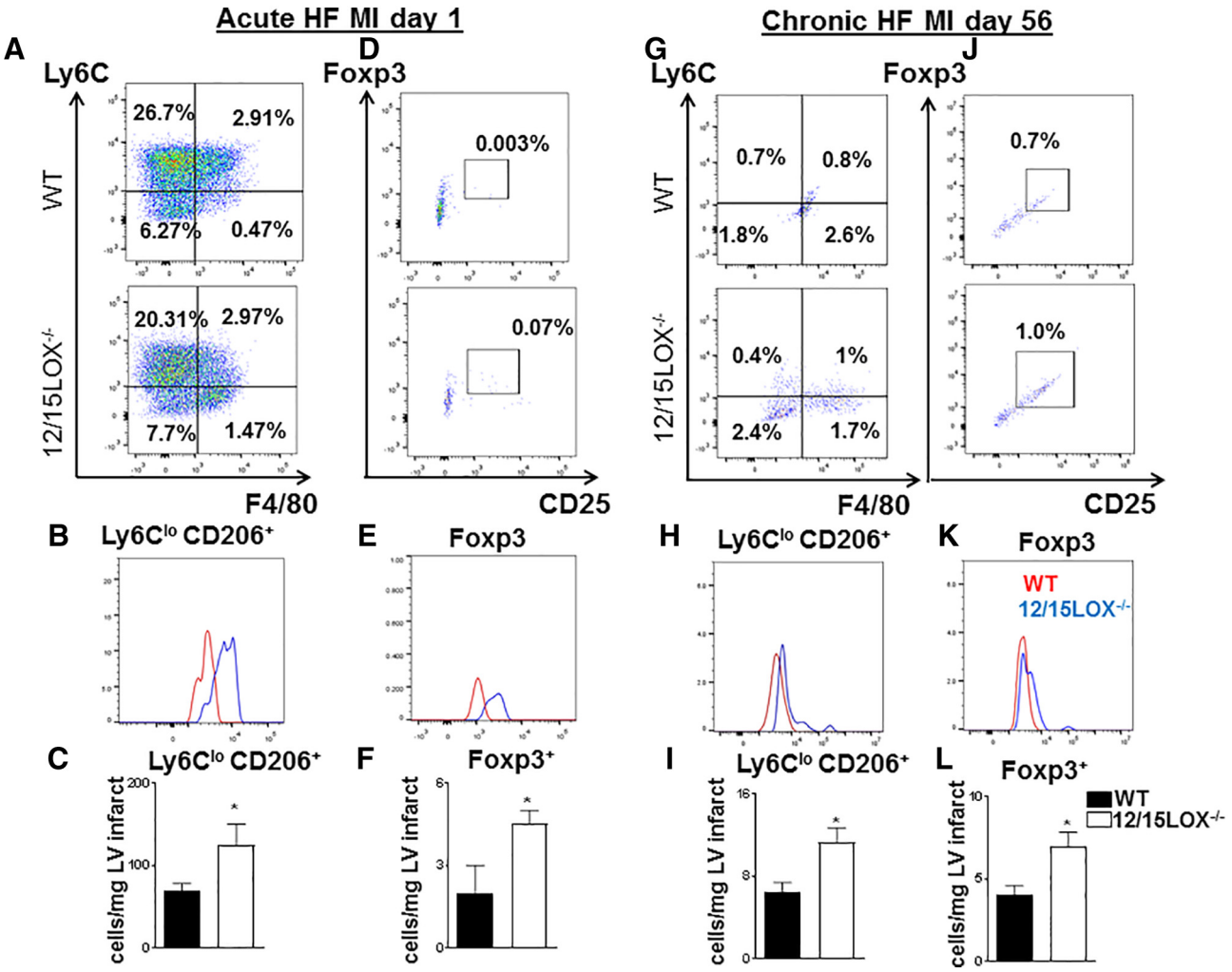

Fig. 7. 12/15LOX$^{-/-}$ increases reparative macrophages in acute HF and Tregs in chronic HF. (A) Representative flow cytometry dot plots showing the macrophage population (F4/80^{+}/Ly6C^{+}) in LV in acute HF in WT and 12/15LOX$^{-/-}$ mice. (B) Histogram representing Ly6C^{lo}/CD206^{+} expression in WT and 12/15LOX$^{-/-}$ mice. (C) Bar graph representing number of Ly6C^{lo}/CD206^{+} cells in LV infarct in acute HF. (D) Representative flow cytometry dot plots showing the Tregs population (Foxp3^{+}/CD25^{+}) in LV in acute HF in WT and 12/15LOX$^{-/-}$ mice. (E) Histogram representing Foxp3^{+} expression in WT and 12/15LOX$^{-/-}$ mice. (F) Bar graph representing number of Foxp3^{+} cells in LV infarct in acute HF. (G) Representative flow cytometry dot plots showing the macrophage population (F4/80^{+}/Ly6C^{+}) in LV in chronic HF in WT and 12/15LOX$^{-/-}$ mice. (H) Histogram representing Ly6C^{lo}/CD206^{+} expression in WT and 12/15LOX$^{-/-}$ mice. (I) Bar graph representing number of Ly6C^{lo}/CD206^{+} cells in LV infarct in chronic HF. (J) Representative flow cytometry dot plots showing the Tregs population (Foxp3^{+}/CD25^{+}) in LV in acute HF in WT and 12/15LOX$^{-/-}$ mice. (K) Histogram representing Foxp3^{+} expression in WT and 12/15LOX$^{-/-}$ mice. (L) Bar graph representing number of Foxp3^{+} cells in LV infarct in chronic HF ($n = 4$; *$p < 0.05$ compared with WT).

spermidine, and decreased levels of phenylalanine and 2-aminoadipic acid as carried over effect from the homeostatic equilibria. In chronic HF mice, the derangement of profound signaling such as hexoses, amino acids, biogenic amines, acylcarnitines, glycerophospholipids, and sphingolipids reached to homeostatic level. Human chronic HF syndrome is complex and heterogeneous with co-medication and co-morbidity that shows decreased levels of amino acids due to a catabolic state, however, in mice, chronic HF does not recapitulate the human chronic HF at metabolic levels due to absence of risk factors such as obesity, hypertension, diabetes, or aging [6,41,42].

4.3. Lipidomic and metabolic milieu regulates leukocyte profiling in acute and chronic HF

The mammalian heart is composed of a cardiac non-myocyte cell pool such as fibroblasts, endothelial cells, B cells, macrophages, dendritic cells, pericytes, Schwann cells, and smooth muscle cells [43,44]. In human and mice, migration of activated splenic leukocytes to the site of injury is required for cardiac healing and the simultaneous orchestration of metabolic programming [18,45,46]. Over-activation or depletion of monocyte/macrophage network impairs cardiac healing with non-resolving inflammation and adverse cardiovascular outcome [18,45,47]. Presented quantitative lipidome in the infarcted heart and plasma metabolome in acute HF provides evidence that activated leukocyte biosynthesize SPMs and cypoxins that offer a unique chemical milieu which is essential for macrophage reparative phenotype and 'get-out' signals to leukocytes after completion of the phagocytic program [17,47]. Impaired leukocyte kinetics due to risk factors such as aging, obesity, or altered lipidome, microbiome, or metabolome milieu due to co-medication such as chemotherapeutics like doxorubicin or pain-killers (non-steroidal anti-inflammatory drugs) alter the leukocyte density and function to develop non-resolving inflammation [24,48–50].

5. Study limitations and clinical perspective

The presented temporal outcome of lipidome and metabolome performed in young and risk free male mice has some limitations since the bioactive lipid species and metabolites signals differ with interventional therapies/surgery, co-morbidity such as obesity, hypertension, diabetes, and aging which is common in HF patients [14,24,48–52]. Additional studies are essential to define the temporal lipid mediators and metabolites in females, cardiac injury in large animal models, or aging animals,

and different strains of mice to determine conservation and reproducibility in acute pre-HF and chronic HF across species. Future studies are required in response to a specific therapy/surgery to define the acute and chronic lipidomic and metabolic signatures, whether that could serve in prevention, prognostics, precision, and personalized medicine in HF patients.

In summary, provided temporal results of leukocyte trafficking, lipidomic, and metabolic signaling shows translational value to define survivor versus non-survivor with diagnostic and prognostic limits in acute and chronic HF. Future studies focused on metabolic and lipidomic signatures are warranted to validate the clinical utility for HF patients.

Supplementary data to this article can be found online at https://doi.org/10.1016/j.metabol.2019.04.011.

Acknowledgement

This work was supported in part by National Institutes of Health [AT006704 and HL132989] and The University of Alabama at Birmingham (UAB) Pittman scholar award to G.V.H., American Heart Association postdoctoral fellowship [POST31000008] to V.K. We thank the Wayne State Lipidomics Core (Dr. Krishna Rao Maddipati), Dr. Helen Karuso (BIOCRATES Inc.), and the Duke University School of Medicine for the use of the Proteomics and Metabolomics Shared Resource, which provided analytical services.

Conflict of interest

None.

References

[1] Taegtmeyer H, Lubrano G. Rethinking cardiac metabolism: metabolic cycles to refuel and rebuild the failing heart. F1000Prime Rep 2014;6:90.
[2] Taegtmeyer H, Goodwin GW, Doenst T, Frazier OH. Substrate metabolism as a determinant for postischemic functional recovery of the heart. Am J Cardiol 1997;80:3A–10A.
[3] Batch BC, Shah SH, Newgard CB, Turer CB, Haynes C, Bain JR, et al. Branched chain amino acids are novel biomarkers for discrimination of metabolic wellness. Metabolism 2013;62:961–9.
[4] Halade GV, Kain V. Obesity and cardiometabolic defects in heart failure pathology. Compr Physiol 2017;7:1463–77.
[5] McGarrah RW, Crown SB, Zhang GF, Shah SH, Newgard CB. Cardiovascular metabolomics. Circ Res 2018;122:1238–58.
[6] Ikegami R, Shimizu I, Yoshida Y, Minamino T. Metabolomic analysis in heart failure. Circ J 2017;82:10–6.
[7] Halade GV, Kain V, Ingle KA. Heart functional and structural compendium of cardiosplenic and cardiorenal networks in acute and chronic heart failure pathology. Am J Physiol Heart Circ Physiol 2018;314:H255-H67.
[8] Emami H, Singh P, MacNabb M, Vucic E, Lavender Z, Rudd JH, et al. Splenic metabolic activity predicts risk of future cardiovascular events: demonstration of a cardiosplenic axis in humans. JACC Cardiovasc Imaging 2015;8:121–30.
[9] Ponikowski P, Anker SD, AlHabib KF, Cowie MR, Force TL, Hu S, et al. Heart failure: preventing disease and death worldwide. ESC Heart Fail 2014;1:4–25.
[10] Cahill TJ, Kharbanda RK. Heart failure after myocardial infarction in the era of primary percutaneous coronary intervention: mechanisms, incidence and identification of patients at risk. World J Cardiol 2017;9:407–15.
[11] Neubauer S. The failing heart—an engine out of fuel. N Engl J Med 2007;356:1140–51.
[12] Kostis JB. Treatment of hypertension in older patients: an updated look at the role of calcium antagonists. Am J Geriatr Cardiol 2003;12:319–27.
[13] Yancy Clyde W, Jessup M, Bozkurt B, Butler J, Casey Donald E, Drazner Mark H, et al. ACCF/AHA guideline for the management of heart failure: executive summary. Circulation 2013;128:1810–52.
[14] van Riet EE, Hoes AW, Wagenaar KP, Limburg A, Landman MA, Rutten FH. Epidemiology of heart failure: the prevalence of heart failure and ventricular dysfunction in older adults over time. A systematic review. Eur J Heart Fail 2016;18:242–52.
[15] Cheng ML, Wang CH, Shiao MS, Liu MH, Huang YY, Huang CY, et al. Metabolic disturbances identified in plasma are associated with outcomes in patients with heart failure: diagnostic and prognostic value of metabolomics. J Am Coll Cardiol 2015;65:1509–20.
[16] Halade GV, Kain V, Ingle KA, Prabhu SD. Interaction of 12/15-lipoxygenase with fatty acids alters the leukocyte kinetics leading to improved postmyocardial infarction healing. Am J Physiol Heart Circ Physiol 2017;313:H89-102.
[17] Kain V, Ingle KA, Kabarowski J, Barnes S, Limdi NA, Prabhu SD, et al. Genetic deletion of 12/15 lipoxygenase promotes effective resolution of inflammation following myocardial infarction. J Mol Cell Cardiol 2018;118:70–80.
[18] Halade GV, Norris PC, Kain V, Serhan CN, Ingle KA. Splenic leukocytes define the resolution of inflammation in heart failure. Sci Signal 2018;11.
[19] Adel S, Karst F, Gonzalez-Lafont A, Pekarova M, Saura P, Masgrau L, et al. Evolutionary alteration of ALOX15 specificity optimizes the biosynthesis of antiinflammatory and proresolving lipoxins. Proc Natl Acad Sci U S A 2014;510:92–101.
[20] Serhan CN. Pro-resolving lipid mediators are leads for resolution physiology. Nature 2014;510:92–101.
[21] Lindsey ML, Bolli R, Canty Jr JM, Du XJ, Frangogiannis NG, Frantz S, et al. Guidelines for experimental models of myocardial ischemia and infarction. Am J Physiol Heart Circ Physiol 2018;314:H812-H38.
[22] Ma Y, Halade GV, Zhang J, Ramirez TA, Levin D, Voorhees A, et al. Matrix metalloproteinase-28 deletion exacerbates cardiac dysfunction and rupture after myocardial infarction in mice by inhibiting M2 macrophage activation. Circ Res 2013;112:675–88.
[23] Menning A, Walter A, Rudolph M, Gashaw I, Fritzemeier KH, Roese L. Granulocytes and vascularization regulate uterine bleeding and tissue remodeling in a mouse menstruation model. PLoS One 2012;7:e41800.
[24] Halade GV, Kain V, Black LM, Prabhu SD, Ingle KA. Aging dysregulates D- and E-series resolvins to modulate cardiosplenic and cardiorenal network following myocardial infarction. Aging (Albany NY) 2016;8:2611–34.
[25] Siskos AP, Jain P, Romisch-Margl W, Bennett M, Achaintre D, Asad Y, et al. Interlaboratory reproducibility of a targeted metabolomics platform for analysis of human serum and plasma. Anal Chem 2017;89:656–65.
[26] Nandania J, Peddinti G, Pessia A, Kokkonen M, Velagapudi V. Validation and automation of a high-throughput multitargeted method for semiquantification of endogenous metabolites from different biological matrices using tandem mass spectrometry. Metabolites 2018;8.
[27] Zordoky BN, Sung MM, Ezekowitz J, Mandal R, Han B, Bjorndahl TC, et al. Metabolomic fingerprint of heart failure with preserved ejection fraction. PLoS One 2015;10:e0124844.
[28] Taegtmeyer H, Young ME, Lopaschuk GD, Abel ED, Brunengraber H, Darley-Usmar V, et al. Assessing cardiac metabolism: a scientific statement from the American Heart Association. Circ Res 2016;118:1659–701.
[29] Burr GO, Burr MM. Nutrition classics from the journal of biological chemistry 82:345-67, 1929. A new deficiency disease produced by the rigid exclusion of fat from the diet. Nutr Rev 1973;31:248–9.
[30] Hu S, Wang L, Yang D, Li L, Togo J, Wu Y, et al. Dietary fat, but not protein or carbohydrate, regulates energy intake and causes adiposity in mice. Cell Metab 2018;28:415–31 (e414).
[31] Kain V, Ingle KA, Kachman M, Baum H, Shanmugam G, Rajasekaran NS, et al. Excess omega-6 fatty acids influx in aging drives metabolic dysregulation, electrocardiographic alterations, and low-grade chronic inflammation. Am J Physiol Heart Circ Physiol 2018;314:H160-9.
[32] Norris PC, Serhan CN. Metabololipidomic profiling of functional immunoresolvent clusters and eicosanoids in mammalian tissues. Biochem Biophys Res Commun 2018;504:553–61.
[33] Serhan CN. Treating inflammation and infection in the 21st century: new hints from decoding resolution mediators and mechanisms. FASEB J 2017;31:1273–88.
[34] Serhan CN, Levy BD. Resolvins in inflammation: emergence of the pro-resolving superfamily of mediators. J Clin Invest 2018;128:2657–69.
[35] Robinette CD, Fraumeni Jr JF. Splenectomy and subsequent mortality in veterans of the 1939–45 war. Lancet 1977;2:127–9.
[36] Dennis EA, Norris PC. Eicosanoid storm in infection and inflammation. Nat Rev Immunol 2015;15:511–23.
[37] Werz O, Gerstmeier J, Libreros S, De la Rosa X, Werner M, Norris PC, et al. Human macrophages differentially produce specific resolvin or leukotriene signals that depend on bacterial pathogenicity. Nat Commun 2018;9:59.
[38] Wang TJ, Ngo D, Psychogios N, Dejam A, Larson MG, Vasan RS, et al. 2-Aminoadipic acid is a biomarker for diabetes risk. J Clin Invest 2013;123:4309–17.
[39] Imai Y, Dobrian AD, Morris MA, Taylor-Fishwick DA, Nadler JL. Lipids and immunoinflammatory pathways of beta cell destruction. Diabetologia 2016;59:673–8.
[40] Eming SA, Wynn TA, Martin P. Inflammation and metabolism in tissue repair and regeneration. Science 2017;356:1026–30.
[41] Aquilani R, La Rovere MT, Corbellini D, Pasini E, Verri M, Barbieri A, et al. Plasma amino acid abnormalities in chronic heart failure. Mechanisms, potential risks and targets in human myocardium metabolism. Nutrients 2017;9.
[42] Bertero E, Maack C. Metabolic remodelling in heart failure. Nat Rev Cardiol 2018;15:457–70.
[43] Skelly DA, Squiers GT, McLellan MA, Bolisetty MT, Robson P, Rosenthal NA, et al. Single-cell transcriptional profiling reveals cellular diversity and intercommunication in the mouse heart. Cell Rep 2018;22:600–10.
[44] Nahrendorf M. Myeloid cell contributions to cardiovascular health and disease. Nat Med 2018;24:711–20.
[45] Zhou X, Liu XL, Ji WJ, Liu JX, Guo ZZ, Ren D, et al. The kinetics of circulating monocyte subsets and monocyte-platelet aggregates in the acute phase of ST-elevation myocardial infarction: associations with 2-year cardiovascular events. Medicine (Baltimore) 2016;95:e3466.
[46] O'Neill LAJ, Kishton RJ, Rathmell J. A guide to immunometabolism for immunologists. Nat Rev Immunol 2016;16:553–65.
[47] Tourki B, Halade G. Leukocyte diversity in resolving and nonresolving mechanisms of cardiac remodeling. FASEB J 2017;31:4226–39.
[48] Jadapalli JK, Wright GW, Kain V, Sherwani MA, Sonkar R, Yusuf N, et al. Doxorubicin triggers splenic contraction and irreversible dysregulation of COX and LOX that alters the inflammation-resolution program in the myocardium. Am J Physiol Heart Circ Physiol 2018;315:H1091-H100.
[49] Halade GV, Kain V, Wright GM, Jadapalli JK. Subacute treatment of carprofen facilitate splenocardiac resolution deficit in cardiac injury. J Leukoc Biol 2018;104:1173–86.

[50] Kain V, Van Der Pol W, Mariappan N, Ahmad A, Eipers P, Gibson DL, et al. Obesogenic diet in aging mice disrupts gut microbe composition and alters neutrophil:lymphocyte ratio, leading to inflamed milieu in acute heart failure. FASEB J 2019: fj201802477R.
[51] Pickens CA, Sordillo LM, Zhang C, Fenton JI. Obesity is positively associated with arachidonic acid-derived 5- and 11-hydroxyeicosatetraenoic acid (HETE). Metabolism 2017;70:177–91.
[52] Werner M, Jordan PM, Romp E, Czapka A, Rao Z, Kretzer C, et al. Targeting biosynthetic networks of the proinflammatory and proresolving lipid metabolome. FASEB J 2019:fj201802509R.